

TABLE II

EXPERIMENTAL VERSUS SIMULATED RESULTS FOR OP-AMP WITH CAPACITIVE DIVIDERS AT ITS INPUT TERMINALS (ATTENUATION FACTOR $A_{tt} = 6$)

	Simulation	Experimental
Minimum V_{DD}	1.15 V	1.1 V
Input Range	1.2 V	1.2 V
Output Range	1.2 V	1.2V
Offset	0.2 mV	1 mV
DC Gain	60 dB	-
Phase Margin	70°	70°
GB	5 MHz	5 MHz
PSRR	40dB	-
CMRR	47 dB	-
THD (100 kHz)	0.09 %	0.1 %
Slew Rate	7 V/ μ s	7 V/ μ s
Peak output Current	0.8 mA	-

was not programmed, but they were erased using ultraviolet light while connecting all circuit terminals to ground.

V. CONCLUSION

A scheme for rail-to-rail continuous-time input signal swing using MIFGTs has been proposed. This scheme provides constant g_m . Single-ended and fully differential op-amp architectures based on this scheme and with a novel class-AB output stage have been introduced. The op-amp operates with a single supply voltage of 1.2 V for transistor threshold voltages of 0.85 V. The op-amp has rail-to-rail input and output signal swings, open-loop gain of 60 dB, phase margin of 70°, 5-MHz gain-bandwidth product, and a slew rate of 7 V/ μ s. This has been verified by simulations and experiments with a fabricated test-chip prototype.

REFERENCES

- [1] A. Baschiroto and R. Castello, "A 1-V 1.8-MHz CMOS switched-opamp SC filter with rail-rail output swing," *IEEE J. Solid-State Circuits*, vol. 32, pp. 1979–1996, Dec. 1997.
- [2] A. Baschiroto, R. Castello, and G. P. Montagna, "Active series switch for switched opamp circuits," *Electron. Lett.*, vol. 34, no. 14, pp. 1365–1366, July 1998.
- [3] V. Peluso, P. Vancorenland, M. Steyaert, and W. Sansen, "900 mV differential class AB OTA for switched opamp applications," *Electron. Lett.*, vol. 33, no. 17, pp. 1455–1456, Aug. 14, 1997.
- [4] G. Ferri, W. Sansen, and V. Peluso, "A low voltage fully differential constant-Gm rail-to-rail CMOS operational amplifier," *Analog Integr. Circuits Signal Process.*, vol. 16, pp. 5–15, 1998.
- [5] J. Fonderie, M. M. Maris, E. J. Schnitger, and J. H. Huijsing, "1-V operational amplifier with rail-to-rail input and output ranges," *IEEE J. Solid-State Circuits*, vol. 24, pp. 1551–1559, Dec. 1989.
- [6] J. Ramírez-Angulo, A. Torralba, R. G. Carvajal, and J. Tombs, "Low-voltage CMOS amplifiers with wide input-output swing based on a novel scheme," *IEEE Trans. Circuits Syst. I*, vol. 48, May 2000.
- [7] B. J. Blalock, P. E. Allen, and G. A. Rincón-Mora, "Designing 1-V op amps using standard digital CMOS technology," *IEEE Trans. Circuits Syst. II*, vol. 45, pp. 769–780, July 1998.

- [8] J. H. Huising, K. de Langen, R. Hogervorst, and R. G. H. Eschiazier, "Low-voltage low-power amplifiers with optimized dynamic range and bandwidth," in *Low-Voltage/Low-Power Integrated Circuits and Systems*. Piscataway, NJ: IEEE Press, 1999, vol. 9, pp. 272–299.
- [9] J. Ramírez-Angulo, S. C. Choi, and G. González-Altamirano, "Low-voltage circuits building blocks using multiple-input floating-gate transistors," *IEEE Trans. Circuits Syst. I*, vol. 42, pp. 971–974, Nov. 1995.
- [10] J. Ramírez-Angulo, "Ultracompact low-voltage analog CMOS multiplier using multiple input floating gate transistors," in *Proc. Eur. Solid State Circuits Conf.*, Neuchatel, Switzerland, May 11–13, 1996, pp. 99–103.
- [11] C. Yu and R. L. Geiger, "Very low-voltage operational amplifiers using floating-gate MOS transistors," in *Proc. IEEE Int. Symp. Circuits and Systems*, vol. II, Chicago, IL, May 3–6, 1993, pp. 1152–1155.
- [12] Y. Berg, D. T. Wisland, and T. S. Lande, "Ultra low-voltage/low-power digital floating-gate circuits," *IEEE Trans. Circuits Syst. II*, vol. 46, pp. 930–941, July 1999.
- [13] K. Yang and A. G. Andreou, "A multiple input differential amplifier based on charge sharing on a floating-gate MOSFET," *Analog Integr. Circuits Signal Process.*, vol. 6, pp. 197–208, 1994.
- [14] J. Ramírez-Angulo, R. G. Carvajal, J. Tombs, and A. Torralba, "A simple technique for op-amp continuous-time 1V operation," *Electron. Lett.*, vol. 35, no. 4, pp. 263–264, Feb. 1999.
- [15] G. González-Altamirano and J. Ramírez-Angulo, "Analog building blocks for a sampled data fast wavelet transform CMOS VLSI implementation," in *Proc. IEEE Int. Conf. Circuits and Systems*, Monterrey, CA, May 31–June 3, 1998, pp. 382–385.
- [16] J. Ramírez-Angulo, G. González-Altamirano, and S. C. Choi, "Modeling multiple-input floating-gate transistors for analog signal processing," in *Proc. 1998 IEEE Int. Conf. Circuits and Systems*, Hong Kong, June 9–12, 1997, pp. 382–385.
- [17] J. Tombs, J. Ramírez-Angulo, R. Carvajal, and A. Torralba, "Integration of multiple-input floating gate transistors into a top-down CAD design flow," in *Proc. Design of Circuits and Integrated Systems*, Mallorca, Nov. 1999, pp. 767–771.
- [18] A. Torralba, R. G. Carvajal, and J. Ramírez-Angulo, "Class AB output stage for low voltage CMOS op-amps with accurate quiescent current control," *Electron. Lett.*, vol. 36, no. 21, pp. 1753–1754, Oct. 2000.

A Second-Order Section Built from Autozeroing Floating-Gate Amplifiers

Paul Hasler, Theron Stanford, and Bradley A. Minch

Abstract—We introduce the autozeroing floating-gate (AFGA) second-order section. We built this second-order filter where the corner frequency and Q are electronically tunable based on a classic filter topology and principles of operational transconductance amplifiers. We built this second-order filter using three AFGAs—our floating-gate amplifier that sets its operating point by the interaction of hot-electron injection and electron tunneling.

Index Terms—AFGA, floating-gate circuits, second-order filters, second-order selections.

Manuscript received March 2000; revised November 2000. This work was supported by the NSF ERC Center for Neuromorphic Systems Engineering. This paper was recommended by Associate Editor T. S. Lande.

P. Hasler is with the School of Electrical and Computer Engineering, Georgia Institute of Technology, Atlanta, GA 30332-0250 USA (e-mail: phasler@ee.gatech.edu).

T. Stanford is with the Department of Electrical Engineering, California Institute of Technology, Pasadena, CA 91125 USA.

B. A. Minch is with the Department of Electrical Engineering, Cornell University, Ithaca, NY 14853 USA.

Publisher Item Identifier S 1057-7130(01)02024-9.

I. INTRODUCTION

We introduce the *autozeroing second-order section* (AutoSOS) in this paper, based upon our earlier work [1]–[4]. The second-order section is the primary element to build higher order filters, both in continuous-time and switch-capacitor circuits. Fig. 1 shows the autozeroing second-order section. This circuit is based on the Diff2 second-order section [5], which in turn is based on a canonical form for a second-order section as a high-gain amplifier with feedback. This circuit uses the autozeroing floating-gate amplifier (AFGA) that we invented previously [1]–[3]. The AFGA does not require any clocking to eliminate offsets, as in switched-capacitor circuits [6], but utilizes an inherent combination of electron tunneling and hot-electron injection currents to eliminate the dc signal.

This paper illustrates how to build higher order filters from AFGAs, as well as proves the feasibility of circuits with multiple floating-gate devices. Using AFGAs as the core filter block merges many of the benefits of switched-capacitor [6] and transconductance-amplifier or operational transconductance amplifier [5] filters. The AFGA-based filters can tune electronically the corner frequencies over many orders of magnitude, as in transconductance amplifiers. Because many of the AFGA's circuit properties—bandpass gain, linear range, and dynamic range—are set by ratios of capacitors, the AFGA-based filters utilize capacitor matching as is done in switched-capacitor filters. Also, the AFGA filters its offsets' $1/f$ noise without resorting to the chopper-stabilizing clocking schemes present in switched-capacitor [6] filters.

We present data from circuits fabricated in a $2\text{-}\mu\text{m}$ n-well Orbit CMOS process available through MOSIS. Typical operating values for V_{tun} were between 33–42 V; those for V_{dd} were 6–12 V. We obtain similar data in the $1.2\text{-}\mu\text{m}$ n-well Orbit CMOS process, but with typical operating values for V_{tun} between 26 and 31 V. For processes with smaller line widths, the typical operating voltages will decrease due to the thinner gate oxide and higher substrate doping.

II. AUTOZEROING FLOATING-GATE AMPLIFIER

Fig. 2 shows the AFGA. The AFGA has four operating regimes that behave similarly for above and below threshold biases. The transfer function of the AFGA is a bandpass with widely separated timeconstants, as seen in Fig. 2(b). Although we could analyze the complete problem, as in [2], we will analyze the high- and low-frequency corner frequencies independently, as is justified by the AFGA data in Fig. 2(b). For an equivalent all-transistor implementation, say, built from capacitively coupled current conveyers (C^4), this wide separation of timescales is not always a good assumption [7], [8]; when the time constants overlap, one already has interesting second-order behavior.

First, the adaptation region of the AFGA is a high-pass filter at low frequencies, which is set by the tunneling and injection currents. The complementary combination of tunneling and hot-electron injection adjusts the floating-gate charge in such a way that the amplifier's output voltage returns to its steady-state value on a slow timescale. We show elsewhere that the low-frequency AFGA behavior is described by [1], [2]

$$C_2 \frac{dV_{\text{out}}}{dt} = -C_1 \frac{dV_{\text{in}}}{dt} + I_{\text{tun}0} \left(\exp\left(-\frac{\Delta V_{\text{out}}}{V_{\text{inj}}}\right) - 1 \right). \quad (1)$$

We derive the frequency response by keeping only the linear terms when we expand the exponentials and taking the Laplace transform

$$\frac{V_{\text{out}}(s)}{V_{\text{in}}(s)} = -\frac{C_1}{C_2} \frac{s\tau_1}{1 + s\tau_1} \quad (2)$$

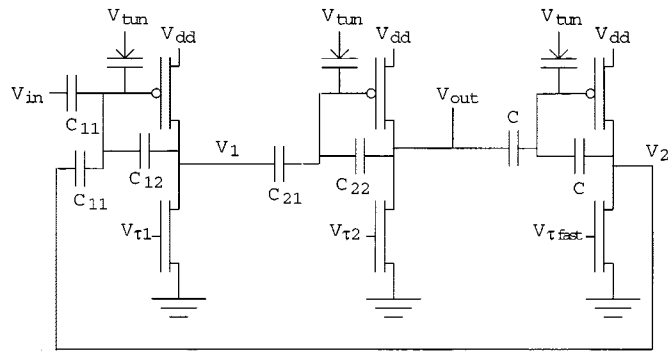


Fig. 1. Circuit diagram of the autozeroing second-order section. This circuit, which is built with three autozeroing amplifiers, shows second-order behavior that is electronically controlled.

where $\tau_1 = C_2 V_{\text{inj}} / I_{\text{tun}0}$. The difference between the tunneling voltage and the pFET's floating-gate voltage sets the equilibrium tunneling current $I_{\text{tun}0}$ and sets the resulting corner frequency.

Second, the integrating region of the AFGA is a low-pass filter at high frequencies, which is set by the nFET bias current. We show elsewhere that the high-frequency AFGA behavior is described by [2], which we write as

$$(C_T C_o - C_2^2) \frac{dV_{\text{fg}}}{dt} = C_1 C_o \frac{dV_{\text{in}}}{dt} + C_2 I_\tau \left(e^{-\kappa \Delta V_{\text{fg}} / U_T} - 1 \right) \quad (3)$$

where C_T is the total capacitance connected to the floating gate ($C_T = C_1 + C_2 + C_w$) and C_o is the total capacitance connected to the output node ($C_o = C_2 + C_L$). For small signals, we linearize (3) by expanding the exponentials for the resulting simplified equation

$$(C_T C_o - C_2^2) \frac{dV_{\text{fg}}}{dt} = C_1 C_o \frac{dV_{\text{in}}}{dt} - \frac{\kappa C_2 I_\tau}{U_T} \Delta V_{\text{fg}}. \quad (4)$$

Again, we derive the frequency response by taking the Laplace transform

$$\frac{V_{\text{out}}}{V_{\text{in}}} = -\frac{C_1}{C_2} \frac{1 - A_h \tau_h s}{1 + \tau_h s} \quad (5)$$

where we define

$$\tau_h = \frac{(C_T C_o - C_2^2) U_T}{\kappa C_2 I_\tau}, \quad A_h = \frac{C_1 C_2}{C_T C_o - C_2^2}. \quad (6)$$

The gain from the input to the output due to capacitive feedthrough is A_h . This transfer function includes the effects of parasitic and load capacitances. The nFET current source sets the bias current and sets the resulting corner frequency.

Third, the amplifier region of the AFGA is between the adaptation and integration regimes. With capacitive feedback, the input signal is amplified by a closed-loop gain approximately equal to $-C_1/C_2$. Fourth, the capacitive feedthrough region occurs at much higher frequencies than the integrating regime, which can be reduced by increasing either C_w or C_L .

The AFGA is always a first-order system even in the presence of parasitic capacitances; therefore, the AFGA is always stable with 90° of phase margin for noninductive loads. Fig. 2(b) shows the frequency response from typical high-gain and unity-gain AFGAs. Any amplifier with resistive feedback is at least a second-order system, but amplifiers with capacitive feedback can be a first-order system. For moderate

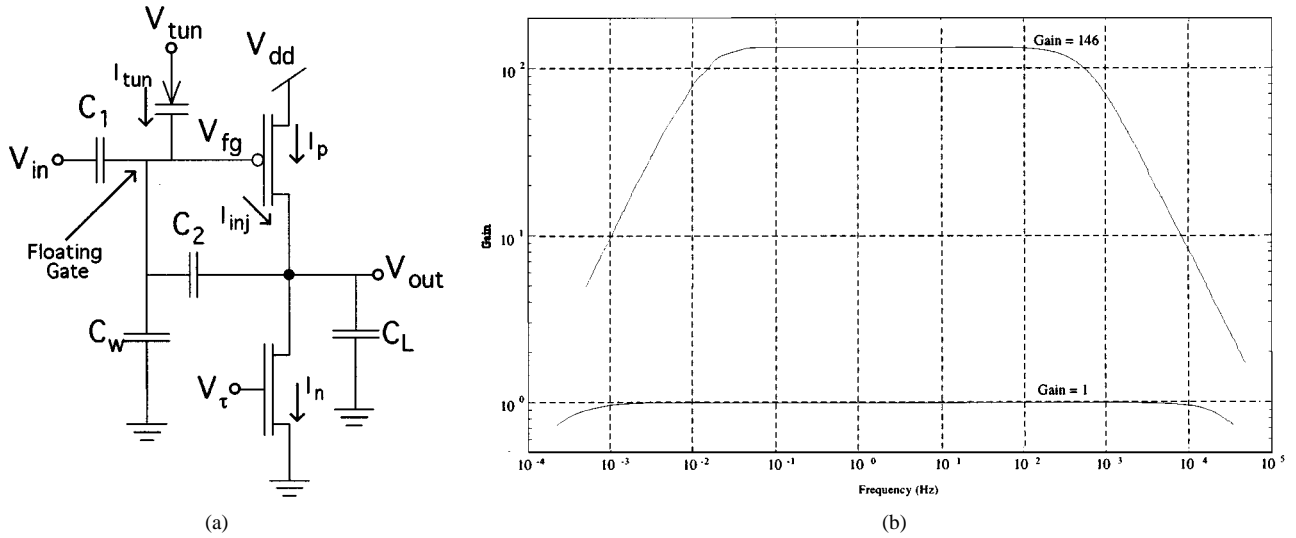


Fig. 2. The autozeroing amplifier that uses the hot-electron injecting pFET. (a) Circuit of the ratio of C_2 to C_1 sets the gain of this inverting amplifier. The nFET is a current source and sets the current through the pFET. Steady state occurs when the injection current (I_{inj}) is equal to the tunneling current (I_{tun}). The capacitance from the floating gate to ground C_w represents both the parasitic and the explicitly drawn capacitances. Increasing C_w will increase the linear input range of the circuit. The capacitance connected to the output terminal C_L is the load capacitance associated with driving other amplifiers. (b) Frequency response for two AFGAs with different gains. For both the high- and low-gain AFGA, $C_1 + C_2$ is approximately constant. For the high-gain AFGA, τ_l is 20 mHz and τ_h is 600 Hz; for the low-gain AFGA, τ_l is 300 μ Hz and τ_h is 40 kHz. The ratio of τ_h and τ_l between the two AFGAs is equal to one-half of the ratio of the gains; the ratio is consistent with a constant $C_1 + C_2$.

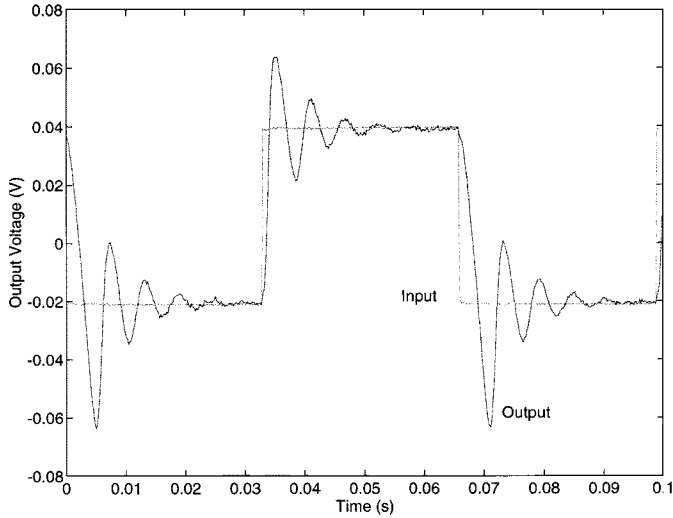


Fig. 3. Response of the autozeroing second-order section due to upgoing and downgoing input steps over a short timescale. The ringing of the output voltage is characteristic of a second-order system.

adaptation rates, the low-frequency time constant remains nearly constant, and any shift is primarily due to trapping in the tunneling oxide.

The AFGA's noise performance is similar in thermal and $1/f$ noise characteristics to a standard MOS amplifier; the tunneling and injection processes do not add appreciable noise to the amplifier. In addition, the adaptation in the AFGA filters the low-frequency noise in the AFGA, an effect that cannot be obtained in a simple amplifier with a blocking capacitor at the input. We can increase the linear range by increasing C_w and the dynamic range by increasing either C_w and/or C_L [2].

III. AUTOZEROING SECOND-ORDER SECTION

Fig. 1 shows the autozeroing second-order section. We will analyze this circuit at both the high- and low-frequency regions of operation. To build a simplified model of the second-order behavior, we assume that $V_2 = -V_{out}$; that is, $V_{\tau fast}$ is set at a bias current much larger

than $V_{\tau 1}$ or $V_{\tau 2}$. By modifying $V_{\tau fast}$, one can achieve a third-order circuit. Similar results are found when using a C^4 based circuit [7] for each AFGA filter.

First, we consider this circuit's operation due to the high-frequency operation of its AFGA circuits. We ignore (for the moment) the floating-gate currents, ignore the capacitive feedthrough effects, and assume that the $V_{\tau 1}$ amplifier's gain is very large. From the AFGA analysis in the previous section, the small-signal model of the two amplifiers based upon (4) is

$$\frac{C_{T1}C_{o1} - C_{12}^2}{C_{12}} \frac{U_T}{\kappa I_{\tau 1}} \frac{dV_1}{dt} = (V_{in} + V_2) \quad (7)$$

$$\frac{C_{T2}C_{o2} - C_{22}^2}{C_{22}} \frac{U_T}{\kappa I_{\tau 2}} \frac{dV_{out}}{dt} = (V_1 + V_{out}) \quad (8)$$

where C_{T1} , C_{T2} are the total capacitances connected to each floating gate including capacitors not drawn in Fig. 1; C_{o1} , C_{o2} are the total capacitances connected to each output node including capacitors not drawn in Fig. 1; and C_{12} , C_{22} are the feedback capacitors from floating gate to output. By defining

$$\tau_1 = \frac{C_{T1}C_{o1} - C_{12}^2}{C_{12}} \frac{U_T}{\kappa I_{\tau 1}} \quad \text{and} \quad \tau_2 = \frac{C_{T2}C_{o2} - C_{22}^2}{C_{22}} \frac{U_T}{\kappa I_{\tau 2}} \quad (9)$$

we solve for the transfer function from V_{in} to V_{out} as

$$\frac{V_{out}(s)}{V_{in}(s)} = \frac{1}{1 + s\tau_1 + s^2\tau_1\tau_2}. \quad (10)$$

From the canonical form for the second-order section, we find that [5]

$$\tau = \sqrt{\tau_1\tau_2}, \quad \text{and} \quad Q = \sqrt{\tau_1/\tau_2}. \quad (11)$$

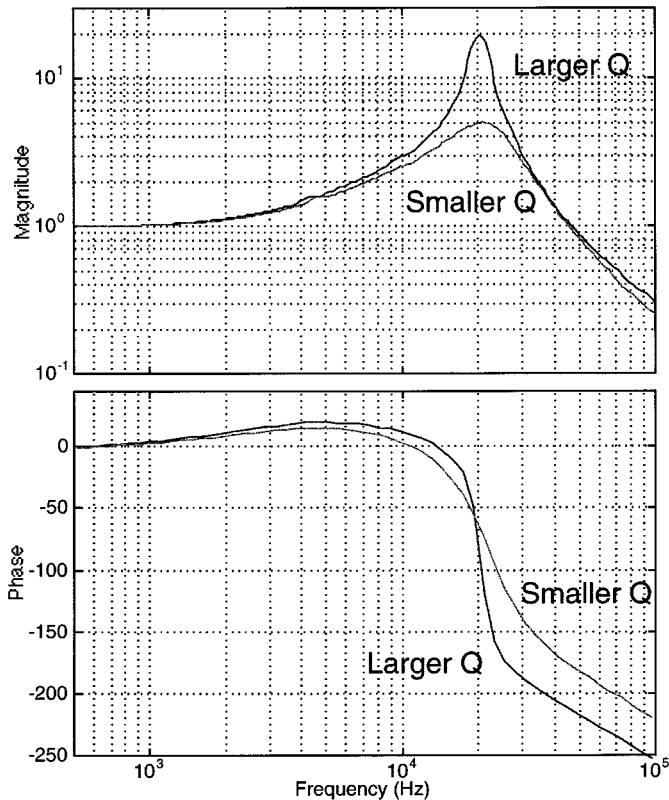


Fig. 4. Frequency response of an AutoSOS for two different bias current settings. The larger Q case is for $V_{\tau 1} = 0.717$ V and $V_{\tau 2} = 0.597$ V, and the smaller Q case is for $V_{\tau 1} = 0.677$ V and $V_{\tau 2} = 0.637$ V. In both cases, we changed the bias current from the model of τ and Q such that the τ of the circuit would remain constant. The effect of capacitive feedthrough for the amplifiers associated with $V_{\tau 1}$ and $V_{\tau 2}$ only starts to appear at the high-frequency end of this data.

Fig. 3 shows the step response of this autozeroing second-order section. The data show the characteristic ringing behavior of a second-order system; changing $V_{\tau 1}$ and $V_{\tau 2}$ changes τ and Q , as predicted from (11).

Fig. 4 illustrates how the frequency response changes by electronically changing the τ_1 and τ_2 values in an AutoSOS; Fig. 4 shows the frequency response for two different values of τ_1 and τ_2 . We tuned these values such that the product of $\tau_1 \tau_2$, and therefore τ , remained constant. In these curves, one sees an initial 20 dB/decade increase just before the Q peak in both responses due to the cutoff frequency of the third amplifier, and this effect increases the amplitude at the Q peak. This response is typical of the V_1 node in an ideal second-order section. The capacitive feedthrough in the third amplifier limits the bandwidth of this effect. The high-frequency phase lag greater than 180° occurs because we are using three amplifiers to build a second-order system.

Fig. 5 shows the frequency response of the first and second harmonics from identical AutoSOSs except with different drawn sizes of C_w (C_w is the capacitance from floating gate to V_{dd}) in all three AFGAs while keeping all other capacitances constant. The second harmonic dominates the distortion of the AFGAs because our nonlinearities arise from subtracting exponential functions from constants and therefore the distortion of the AutoSOS. The maximum second-harmonic distortion is nearly at half of the section's corner frequency. Increasing C_w has three effects.

- 1) τ decreases linearly with increasing C_w (which increases C_T).
- 2) The capacitive feedthrough from input to output decreases.

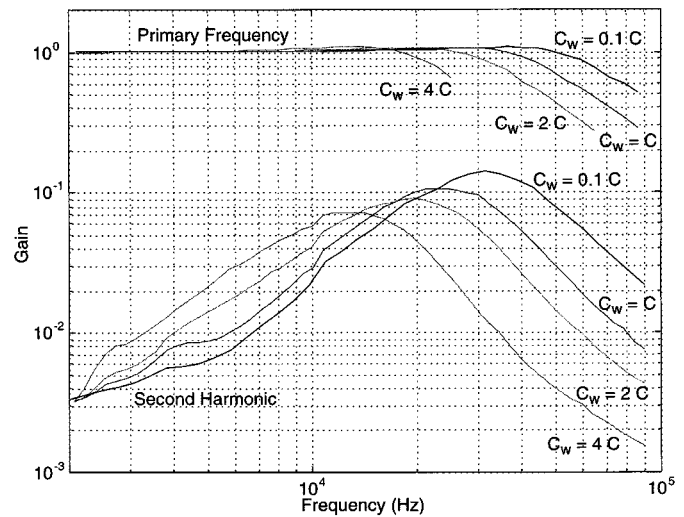


Fig. 5. Frequency response of the first and second harmonic components of AutoSOSs for four different values of C_w in all three AFGAs. C_w is the capacitance from floating gate to V_{dd} and therefore increases the overall value of C_T . Also, $C_{11} = C_{21} = C_{22}$ remained constant for all measurements. The AutoSOS was biased to have a Q slightly greater than one. The input amplitude was much larger than the second AFGA's linear range. We see that increasing C_w linearly increases τ but linearly decreases the peak second-harmonic response.

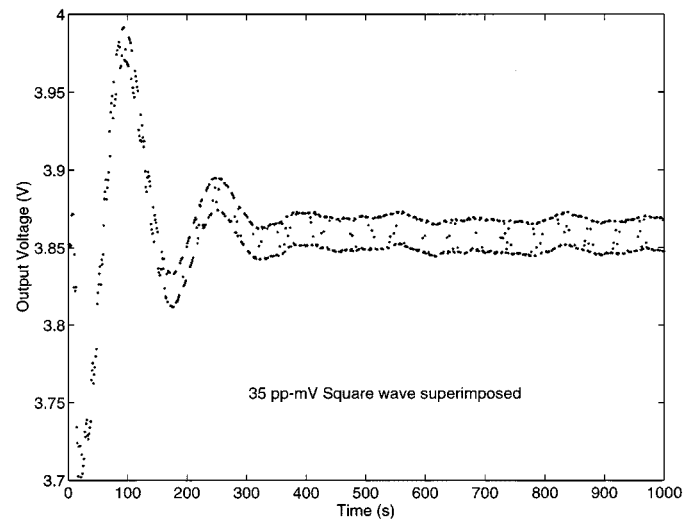


Fig. 6. Response of the autozeroing second-order section due to an ongoing input steps over a long timescale. A 1-Hz square wave was superimposed on the input signal and is preserved throughout the relaxation. This ringing behavior proves that the circuit exhibits at least second-order behavior from the AFGA corner frequencies set by the floating-gate currents.

- 3) Second-harmonic distortion decreases linearly with increasing C_w , because the signal level at the floating gate is decreased by the resulting capacitive voltage divider.

Therefore, as in the AFGAs [2], the AutoSOS's linear range and dynamic range increase linearly, and peak distortion decreases linearly with increasing C_w .

IV. LOW-FREQUENCY TIME-RESPONSE BEHAVIOR

The AFGA also has a high-pass cutoff at low frequencies. Therefore, coupling three of these stages with negative feedback may also produce second- or third-order behavior at low frequencies. Using small signal

models, we can write three equations for the three AFGAs around the low-frequency corners as (assume for clarity that $C = C_{11} = C_{21} = C_{22}$)

$$\begin{aligned}\frac{dV_2}{dt} &= -\frac{dV_{in}}{dt} - \frac{I_{tun01}}{V_{inj}C} \Delta V_1 \\ \frac{dV_1}{dt} &= -\frac{dV_{out}}{dt} - \frac{I_{tun02}}{V_{inj}C} \Delta V_{out} \\ \frac{dV_2}{dt} &= -\frac{dV_{out}}{dt} - \frac{I_{tun03}}{V_{inj}C} \Delta V_2\end{aligned}\quad (12)$$

where the equilibrium tunneling currents I_{tun01} , I_{tun02} , I_{tun03} are set by difference between their respective tunneling and pFET's floating-gate voltages; for clarity, C_{12} is assumed to be negligible for this analysis. We have ignored the passband regime for the first amplifier because it has a small effect on the low-frequency dynamics, as was true for deriving the high-frequency dynamics. Laplace transforming these equations, we solve the coupled equations for the following resulting V_2 equation:

$$V_2 = -\frac{V_{in}}{1 + \frac{I_{tun01}}{sCV_{inj}} + \frac{I_{tun01}(I_{tun02} + I_{tun03})}{s^2C^2V_{inj}^2}} + O(3)\quad (13)$$

By comparing this equation to the low-frequency equivalent of a second-order section

$$\frac{V_2(s)}{V_{in}(s)} = \frac{1}{1 + \frac{1}{Qs\tau} + \frac{1}{s^2\tau^2}}\quad (14)$$

we get an effective τ and Q as

$$\begin{aligned}\tau &= \frac{CV_{inj}}{\sqrt{tun01(I_{tun02} + I_{tun03})}} \\ Q &= \sqrt{\frac{I_{tun02} + I_{tun03}}{I_{tun01}}}\end{aligned}\quad (15)$$

Fig. 6 shows the step response at a very slow timescale. The damped oscillatory behavior is due to the corner frequencies set by the tunneling currents and is indicative of at least a second-order circuit. The low-frequency filtering in this circuit provides the basis for the design of integrated filters operating at very low frequencies less than 10 Hz to frequencies below 1 μ Hz.

REFERENCES

- [1] P. Hasler, B. A. Minch, C. Diorio, and C. Mead, "An autozeroing amplifier using pFET hot-electron injection," in *Proc. Int. Symp. Circuits and Systems*, vol. 3, Atlanta, GA, 1996, pp. 325–328.
- [2] P. Hasler, B. A. Minch, and C. Diorio, "An autozeroing floating-gate amplifier," *IEEE Trans. Circuits Syst. II*, vol. 48, pp. 74–82, Jan. 2001.
- [3] P. Hasler, "Foundations of learning in analog VLSI," Ph.D. dissertation, California Institute of Technology, Pasadena, 1997.
- [4] P. Hasler, T. Stanford, B. A. Minch, and C. Diorio, "An autozeroing floating-gate second-order section," in *Proc. IEEE Int. Symp. Circuits and Systems*, Monterey, CA, 1998, pp. 351–354.
- [5] C. Mead, *Analog VLSI and Neural Systems*. Reading, MA: Addison-Wesley, 1989.
- [6] R. Gregorian and G. C. Temes, *Analog MOS Integrated Circuits for Signal Processing*. New York: Wiley-Interscience, 1986.
- [7] P. Hasler, M. Kucic, and B. A. Minch, "A transistor-only circuit model of the autozeroing floating-gate amplifier," in *Proc. IEEE Midwest Symp. Circuits and Systems*, Las Cruces, NM, 1999.
- [8] M. Kucic, A. Low, P. Hasler, and J. Neff, "A programmable continuous-time floating-gate Fourier processor," *IEEE Trans. Circuits Syst. II*, vol. 48, pp. 90–99, Jan. 2001.